Journal of Alloys and Compounds 960 (2023) 170793

Contents lists available at ScienceDirect

Journal of Alloys and Compounds

journal homepage: www.elsevier.com/locate/jalcom

Multi-objective optimization for high-performance Fe-based metallic glasses via machine learning approach

Yu-Xing Zhang [a,b], She-Juan Xie [a], Wei Guo [c], Jun Ding [d], Leong Hien Poh [e,*], Zhen-Dong Sha [a,f,**]

[a] State Key Laboratory for Strength and Vibration of Mechanical Structures, School of Aerospace Engineering, Xi'an Jiaotong University, Xi'an 710049, China
[b] China Electronics Technology Group Corporation, 52nd Research Institute, Hang'zhou 310000, China
[c] State Key Lab of Materials Processing and Die & Mould Technology, Huazhong University of Science and Technology, 1037 Luoyu Road, Wuhan 430074, China
[d] Center for Alloy Innovation and Design, State Key Laboratory for Mechanical Behavior of Materials, Xi'an Jiaotong University, Xi'an 710049, China
[e] Department of Civil and Environmental Engineering, National University of Singapore, 1 Engineering Drive 2, E1A-07-03, Singapore 117576, Singapore
[f] State Key Laboratory of Nonlinear Mechanics, Institute of Mechanics, Chinese Academy of Sciences, Beijing 100190, China

ARTICLE INFO

Article history:
Received 16 February 2023
Received in revised form 7 May 2023
Accepted 29 May 2023
Available online 30 May 2023

Keywords:
Fe-based metallic glass
Machine learning
Critical casting size
Saturation magnetization
Plasticity

ABSTRACT

Fe-based metallic glasses (MGs) are a class of promising soft magnetic materials that have received great attention in transformer industries. However, it is challenging to achieve a balance between saturation magnetization (B_s), glass-forming ability and plasticity due to their contradictory correlations in Fe-based MGs, which severely hinders the development of new Fe-based MGs with advanced performances. Inspired by the significant development in machine learning technology, we herein propose a multi-objective optimization strategy to search for Fe-based MGs with optimal combinations of critical casting size (D_{max}), B_s, and plasticity. The objective functions are built in combination with neural network models for predicting D_{max} and B_s, as well as empirical formula for plasticity. The effect of number of hidden layers is investigated and the dropout regularization method employed to improve the prediction performance. Our results show that the predictions of B_s and D_{max} by using alloy composition as the sole input perform well, as evidenced by their r^2 values of 0.963 and 0.874, respectively. Multi-objective optimization based on the genetic algorithm is executed to obtain the Pareto front and Pareto-optimal solutions. The Pareto-optimal alloys predicted for the $Fe_{83}C_1B_xSi_yP_{16-x-y}$ and $Fe_xCo_yNi_{72-x-y}B_{19.2}Si_{4.8}Nb_4$ systems are in good agreement with those reported in experiments. This work thus showcases potential applications for the design of high-performance Fe-MGs against conflicting objectives.

1. Introduction

Metallic glasses (MGs) have generated great interest because of their unique and unconventional mechanical, physical and chemical properties such as profound elastic strain limit (~2%), high mechanical strength (~2 GPa), excellent corrosion resistance, and extreme biocompatibility without cytotoxicity [1–4]. Among the MGs, Fe-based MGs possess high saturation magnetization (B_s) and low coercive force. This class of MGs has thus attracted more attention for industrialization and commercialization purposes, and has been widely applied as transformer cores to replace traditional Si-steel [5–8]. However, two remaining challenges in utilizing Fe-based soft magnetic MGs for industrial applications are their low glass-forming ability (GFA) and very poor plasticity (< 0.5%) at room temperature [4,9–11]. It is therefore imperative to develop Fe-based MGs with high B_s, robust GFA and superior plasticity.

However, it is difficult to strike a balance between B_s, GFA and plasticity due to their contradictory relationships in Fe-based MGs. Typically, the B_s increases with Fe content. The additions of suitable quantities of transition metals and metalloids can improve the GFA, while a reduced Fe content leads to a decrease in B_s [12,13]. Moreover, the electronic interactions between Fe and metalloids reduce the effective magneton number at the same time [13–16]. Note also that a relatively high content of metalloids will deteriorate the plasticity [17]. Therefore, it is important to find an optimum Fe-based MG composition to achieve an exceptional combination of high B_s with improved GFA and plasticity.

* Corresponding author.
** Corresponding author at: State Key Laboratory for Strength and Vibration of Mechanical Structures, School of Aerospace Engineering, Xi'an Jiaotong University, Xi'an 710049, China.
E-mail addresses: leonghien@nus.edu.sg (L.H. Poh), zhendongsha@mail.xjtu.edu.cn (Z.-D. Sha).

https://doi.org/10.1016/j.jallcom.2023.170793
0925-8388/

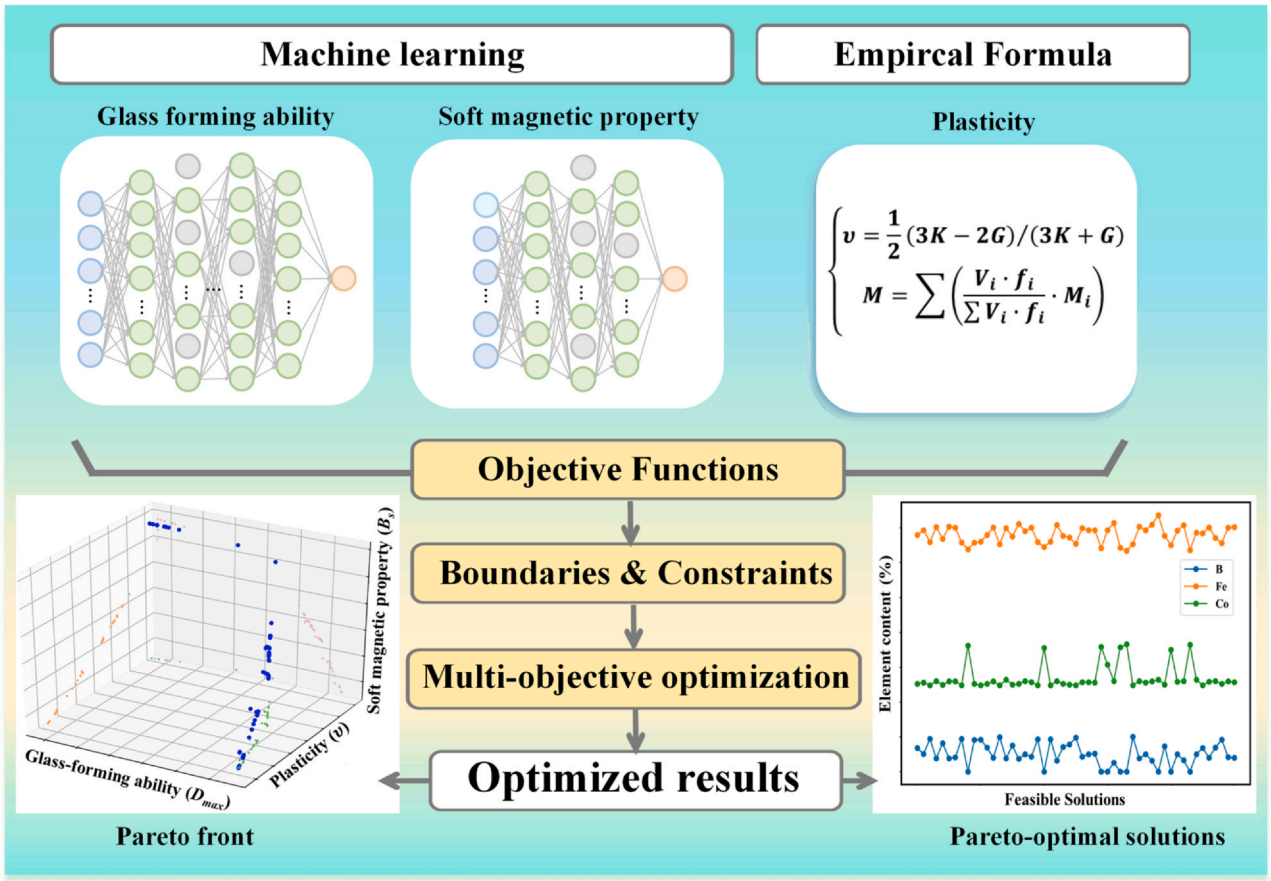

Fig. 1. Schematic illustration of the search strategy for high-performance Fe-based MGs.

While a heuristic microalloying strategy can result in the development of MGs with desired properties, it is a time-consuming and costly iterative process [14,18–23]. The development and adoption of machine learning (ML) methods has accelerated the discovery of high-performance materials [24–26]. ML has the potential to accurately predict materials properties at a low computational cost [27–38], even for multi-element alloys like MGs, which exhibit strong composition-dependent behavior. However, it is still a major challenge to simultaneously optimize multi-objective problems. One promising scheme is the metaheuristic method, including the genetic algorithm (GA), ant colony optimization (ACO), particle swarm optimization (PSO), and simulated annealing methods. Metaheuristic method is able to find near-optimal solutions in complex optimization problems with large variables [39]. For example, García-Carrillo et al. combined artificial neural network (NN) and GA to simultaneously optimize against conflicting properties such as

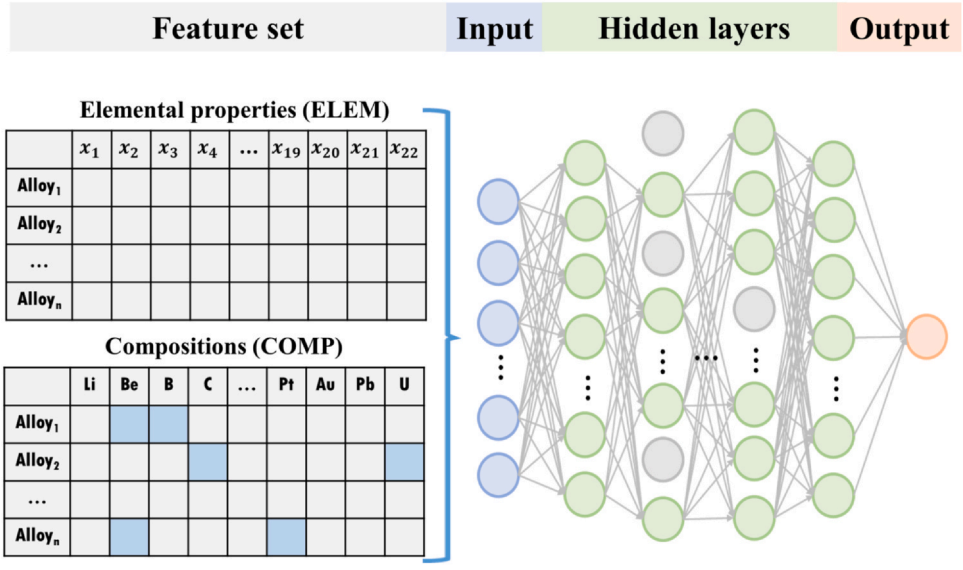

Fig. 2. Schematic illustration of the structure of NN. The gray neurons represent those randomly discarded with a certain probability at each training iteration.

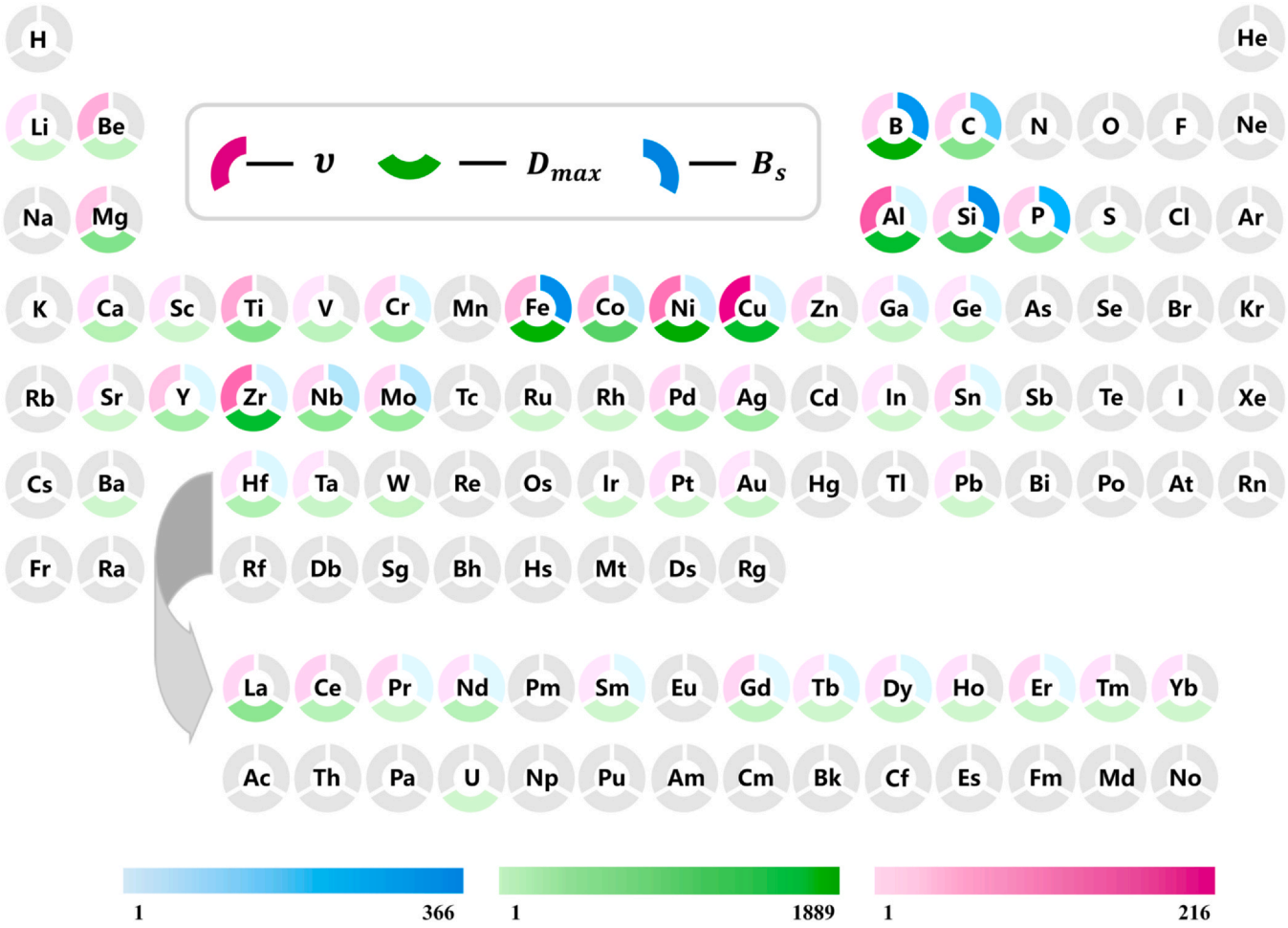

Fig. 3. The number of occurrence of elements presented in the three datasets of D_{max}, B_s, and ν, depicted in terms of the intensity of color fills. For each element, the red fill in the top left segment indicates its presence in the dataset of ν, the blue fill in the top right segment indicates its presence in an alloy for which we have a B_s value, and the green fill in the bottom segment indicates its presence in the dataset of D_{max}. The absence of an element in the dataset is depicted with a gray fill.

thermal and electrical conductivities in polyethylene-carbon particle composites [40].

In the present work, we couple NN and GA to optimize against conflicting objectives (i.e., B_s, GFA, and plasticity) for achieving superior Fe-based MGs. We first build the objective functions for three key properties of Fe-based MGs. Next, a systematic investigation is carried out on the number of hidden layers, dropout regularization method, as well as input feature. Finally, multi-objective optimization based on GA is adopted. The proposed ML framework is validated considering $Fe_{83}C_1B_xSi_yP_{16-x-y}$ and $Fe_xCo_yNi_{72-x-y}B_{19.2}Si_{4.8}Nb_4$ systems, with a view towards potential tailoring of properties for Fe-based MGs.

2. Methods

Our proposed strategy for achieving the desired high-performance Fe-based MGs consists of 3 steps, as summarized in Fig. 1. The first step is to build objective functions that define the relationship between inputs and output variables. Due to the general lack of data on ν values for Fe-based MGs in the literature (less than 60), the empirical criteria for plasticity based on the "rule of mixture" and ν is utilized. The second step is to define the boundaries and constraints that the solution must satisfy in an optimization problem. The final step is to execute multi-objective optimization based on GA and obtain the Pareto front and Pareto-optimal solutions.

2.1. Objective functions

2.1.1. ML model for predicting critical casting size (D_{max}) and B_s

The open source ML framework PYTORCH is utilized to build NN models. NN models implemented with nonlinear activation function can approximate any complex functions [41]. In this study, we employ the rectified linear unit (ReLU) as the nonlinear activation function, as defined by Eq. (1) [42]. In the process of gradient propagation, ReLU may set the outputs of some neurons to 0, leading to sparse activation and better gradient propagation [43].

$$f(x) = \max(0, x) \tag{1}$$

where x is the input value for a neuron unit.

The structure of NN includes the input layer, output layer, and hidden layers, as illustrated in Fig. 2. Dropout regularization method is employed for reducing overfitting in NN, in which the neurons are randomly discarded with a certain probability at each iteration. From the perspective of ensemble learning, each training iteration based on different networks can reduce overfitting and improve the prediction performance [44].

The coefficient of determination (r^2) and root-mean-square error (RMSE) are employed to quantify the performance of NN. r^2 describes how well the NN model predicts the actual values (y_i), and RMSE represents the deviations between predicted and actual values. They are defined as [45]:

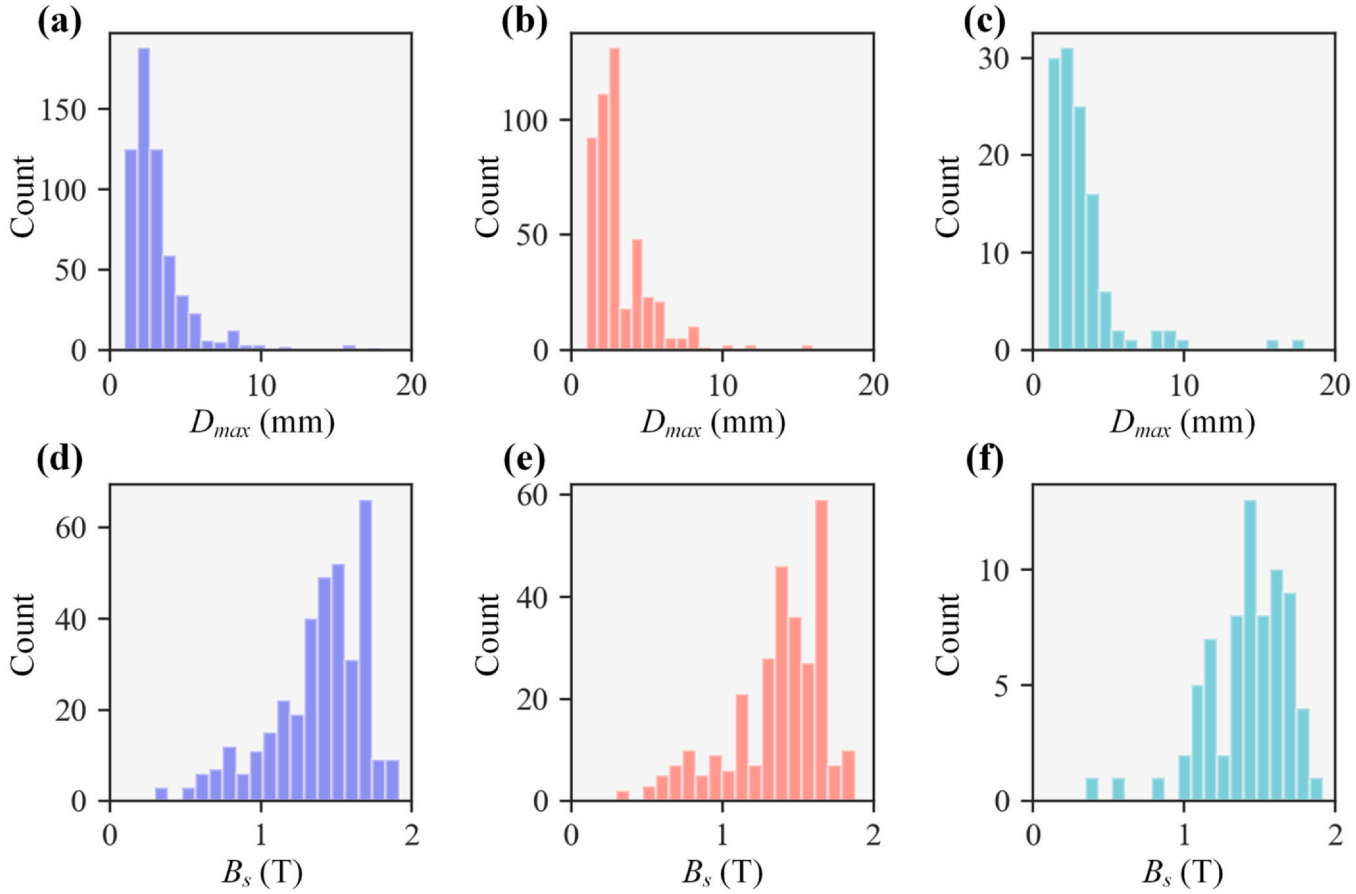

Fig. 4. The distribution of (a-c) D_{max} and (d-f) B_s datasets. The left, middle, and right panels indicate the full dataset, the training set, and the test set, respectively.

$$r^2 = 1 - \frac{\sum_{i=1}^{N}(y_i - \hat{y}_i)^2}{\sum_{i=1}^{N}(y_i - \bar{y})^2} \quad (2)$$

$$\mathrm{RMSE} = \sqrt{\frac{1}{N}\sum_{i=1}^{N}(y_i - \hat{y}_i)^2} \quad (3)$$

where $\bar{y}$ is the average of y_i, and $\hat{y}_i$ is the predicted value. $r^2 = 1$ denotes a perfect match between predictions and actual data. A low RMSE value indicates that the predicted and actual values are close to each other, showing a better accuracy.

2.1.2. Empirical formula of ν for indicating plasticity

Previous studies have reported that MGs exhibit a brittle-to-ductile transition at a critical ν value of 0.31–0.32 [46–48]. ν is calculated by Eq. (4):

$$\nu = \frac{1}{2}(3K - 2G)/(3K + G) \quad (4)$$

where K and G are the bulk modulus and shear modulus, respectively.

Wang has proposed that the elastic constants of MGs can be calculated by the average of the moduli of each constituent element according to the "rule of mixture" [48]. Liu et al. have also proposed a method for precisely calculating the elastic constants based on the base elements of MG [49]. Unfortunately, they did not conclude the parameters used for Fe-based MGs. In the following, the "rule of mixture" proposed by Wang et al. is adopted to calculate the elastic constants of Fe-based MGs, which is defined by [48]:

$$M = \sum\left(\frac{V_i \cdot x_i}{\sum V_i \cdot x_i} \cdot M_i\right) \quad (5)$$

where x_i, V_i and M_i denote the proportion, atomic volume, and modulus of the i-th constituent element, respectively. It should be mentioned that since the metalloid elements (i.e., B, C, P, and Si) only have bulk moduli, the Cauchy relation ($K = 5G/3$) is adopted to determine their assume shear moduli [48].

2.2. Multi-objective optimization

The Genetic and Evolutionary Algorithm toolbox for Python with High Performance (GEATPY) is employed to build the multi-objective optimization model [50]. GA is an optimization method to search for the optimal solution by simulating the process of natural evolution [51]. The basic structure of a GA is as follows. In a certain population size, population individuals undergo crossover, recombination and mutation, and then produce new individuals. This process repeats in different generations. Each individual in the population is assigned a fitness value normally based on its objective function value. Individuals with higher fitness values are more likely to survive. After multiple evolutions, better solutions are obtained. In our work, the evolutionary algorithm using a reference point based on a nondominated sorting approach is employed to search the trade-offs among the conflicting objectives [51,52]. During optimization, the crossover probability and mutation probability are fixed at 0.9 and 0.1, respectively. The population size is set to 100. In our work, Pareto-optimal solutions in multi-objective optimization among the conflicting objectives of GFA, B_s, and plasticity in Fe-based MGs represent the trade-off compositions.

2.3. Datasets

Our datasets are collected from the public handbook and literature [6,12,29,33,35,37,46,48,53–64]. Most of the data about GFA are

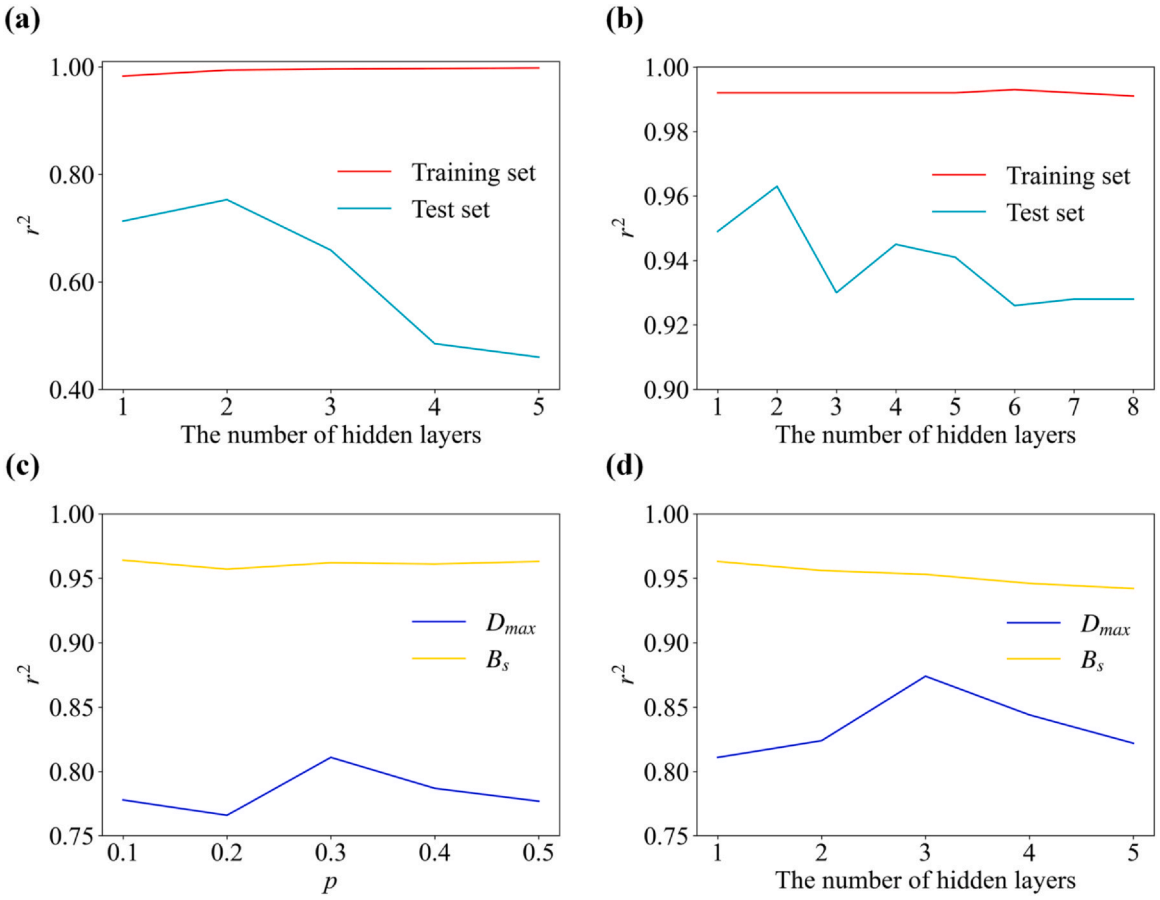

Fig. 5. The r^2 value as a function of the number of hidden layers when predicting (a) D_{max} and (b) B_s without dropout method. (c) The r^2 value as a function of p when fixing the number of hidden layer at 1. (d) The r^2 value as a function of the number of hidden layers when p values are fixed at 0.1 and 0.3 for D_{max} and B_s, respectively.

Table 1
The r^2 values for predicting D_{max} and B_s without and with the dropout method.

Hidden layers	r^2 values without dropout method		r^2 values with dropout method		Change in r^2	
	D_{max}	B_s	D_{max}	B_s	D_{max}	B_s
1	0.713	0.949	0.811	0.963	13.7%	1.5%
2	0.753	0.963	0.824	0.956	9.4%	-0.7%
3	0.659	0.930	0.874	0.953	32.6%	2.3%
4	0.485	0.945	0.844	0.946	74.0%	0.1%
5	0.460	0.941	0.822	0.942	78.7%	0.1%

taken from Samavatian et al. 's work [37], which was dated back to Ward et al.'s work and the Landolt-Bornstein Handbook [29,64]. The datasets of B_s and ν are mainly derived from the work of Lu et al. and Wang [33,48], respectively. Initially, the numbers of data of D_{max}, B_s, and ν are 5689, 366, and 305, respectively. Fig. 3 shows the number of occurrence of each element in the corresponding dataset. In general, our database covers 55 different elements in the periodic table, including metallic and metalloid elements frequently presented in MGs. Besides, the elements in the D_{max} dataset are widely distributed, while those in the B_s and ν datasets are mainly enriched in Fe, B, C, Si and P, and Al, Ni, Cu and Zr, respectively.

At the next step, we rule out some unreasonable data based on two criteria. First, the samples with a proportion of Fe less than 0.3 are deleted due to the fact that an increased Fe content can increase the B_s. Second, samples with $D_{\max} < 1$ mm are also discarded, since they reflect poor GFA. The resulting data size for D_{max}, B_s, and ν is 589, 360, and 21, respectively. Due to the limited dataset, we divide the training set and the test set at a ratio of 8:2. Fig. 4 shows the distribution of D_{max} and B_s data. A skewed distribution with a typical long tail is observed for the D_{max} data, while a normal distribution is observed for the B_s data.

3. Results and discussion

3.1. NN models for predicting D_{max} and B_s

3.1.1. Determination of the structure of NN

In the NN, an increased number of hidden layers generally improves the fitting ability for the training set. However, too many hidden layers may lead to overfitting, especially if the training set contains limited samples. In our work, the dropout regularization method is employed to prevent model overfitting. In order to determine the best NN structure, we systematically study the influence of the number of hidden layers and dropout probability (p) on the prediction accuracy, as shown in Fig. 5.

Fig. 5(a-b) shows the effect of the number of hidden layers when predicting D_{max} and B_s without dropout method. For predicting D_{max} as shown in Fig. 5(a), the r^2 value for the training set increases slightly and reaches the highest value of 0.998 at 5 hidden layers. In contrast, the r^2 value for the test set increase at first and then decreases. The NN with 2 hidden layers exhibits the highest r^2 value of 0.753 for the test set. For predicting B_s as shown in Fig. 5(b), the trend of r^2 is similar to that of D_{max}. Besides, the model performs well on the test set, as evidenced by $r^2 > 0.93$ regardless of the

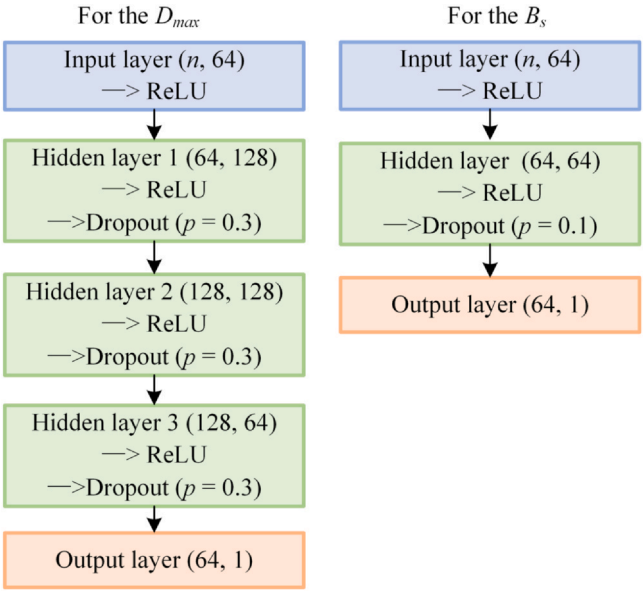

Fig. 6. The adopted NN structure for predicting D_{max} and B_s. n denotes the number of features.

Table 2
The basic elemental properties employed in our work.

The elemental properties		
Atomic mass	Atomic number	Atomic radius
Atomic size difference	Boiling point	Covalent radius
Density	Electrical conductivity	Electron affinity
Electronegativity	First ionization energy	Group
Heat of fusion	Heat of vapourization	Ionic radius
Melting point	Mixing entropy	Period
Specific Heat	Thermal Conductivity	Valence
Volume		

number of hidden layers. It is worth mentioning that a r^2 value of 0.949 is achieved for only one hidden layer.

In order to further improve the prediction performance to avoid overfitting, we next investigate the effect of p with the number of hidden layer fixed at 1, as shown in Fig. 5(c). The r^2 values for D_{max} and B_s reach the highest values when p values are set to be 0.3 and 0.1, respectively. After the determination of p values, we proceed to fix the number of hidden layers for predicting D_{max} and B_s. Fig. 5(d) shows that as the number of hidden layers increases, the r^2 value increases at first and decreases when predicting D_{max}, attaining a maximum value of 0.874 at 2 hidden layers. When predicting B_s, the r^2 value decreases with the number of hidden layers.

Table 1 summarizes the r^2 values as a function of the number of hidden layers and p. It is clearly observed that the prediction performance is greatly improved with the application of the dropout method, especially for predicting D_{max}. For example, when the number of hidden layers is 5, the r^2 value increases by 78.7% from 0.460 to 0.822 after using the dropout method. Similarly, the NN for predicting B_s is also improved slightly after using the dropout method. Furthermore, it is observed that the NN for predicting B_s performs better than that for predicting D_{max}. The r^2 value for predicting B_s is up to 0.963, which is ~10% higher than that of the NN for predicting D_{max}. This is attributed to the imbalanced dataset involved by the limited data in the regime of large D_{max}. From this exercise, it is concluded that the dropout regularization method can improve the prediction accuracy. Fig. 6 shows the final structure of our NN model.

3.1.2. Determination of the input features

The input features are the "material genes" linked with the target material properties. Some previous studies directly used alloy compositions as inputs [35], while others constructed the input features based on the basic properties of elements [28,29,33,58]. To study the effect of different input features on the prediction performance, we consider three kinds of input features including the alloy compositions (COMP), the elemental properties (ELEM), and the combination of alloy compositions and elemental properties (COMP+ELEM).

There are 22 kinds of elemental properties used in this work, as listed in Table 2. Except for the atomic size difference (δ_D), mixing entropy (ΔS), and volume (V), the other elemental properties can be determined using the weighted average formula. For the four highlighted features, they can be calculated as [29,58,65,66]:

$$\delta_D = \sqrt{\sum x_i \left(1 - \frac{r_i}{\bar{r}}\right)^2} \tag{6}$$

$$V = \sum x_i \frac{4}{3}\pi r_i^3 \tag{7}$$

$$\Delta S = -R_g \sum x_i \ln\left(x_i V_i / \sum x_i V_i\right) \tag{8}$$

$$Z = \sum x_i Z_i \tag{9}$$

where x_i, V_i, and r_i represent the proportion, atomic volume, and atomic radius of i-th element, respectively. R_g and $\bar{r}$ denote the gas constant value and the average atomic radius, respectively. Z indicates those elemental properties except for δ_D, ΔS and V.

Fig. 7 shows the predicted D_{max} and B_s against measured D_{max} and B_s based on the three different input features, in which the diagonal line represents perfect prediction. It is clearly seen that the points on Fig. 7(d-f) are closer to the diagonal line than those on Fig. 7(a-c), indicating that the B_s prediction performs much better than D_{max} prediction. Although some outliers in the regime of large D_{max} are observed due to the limited data on large D_{max} in the literature, our approach still demonstrates an improved predictive capability compared with previous studies [28,35,67,68], as discussed in detail below.

Table 3 lists the r^2 and RMSE values of the D_{max} and B_s predictions from three different input features. It is easily observed that the predictions obtained by using COMP as the sole input feature for D_{max} and B_s have the best accuracy, as evidenced by the largest r^2 and the smallest RMSE values. In contrast, the use of ELEM as the sole input feature performs the worst. This may be because the calculation formulas related to ELEM are based on the homogeneous materials that are uniform without irregularities, but MGs display the structural inhomogeneity. Therefore, the use of COMP to predict the D_{max} and B_s of MGs would be more accurate. For predicting B_s, our r^2 value of 0.963 is higher than the values in the work of Lu et al. and Li et al. [33,69]. In addition, the r^2 value of 0.874 for predicting D_{max} is much larger than those reported in most previous studies, for example, 0.61 in the work of Deng et al. [67], and 0.71 in the work of Mastropietro et al. [35]. In term of RMSE, our value is 25.8% lower than the value of 1.2063 mm in the work of Xiong et al. [68].

3.2. Multi-objective optimization of Fe-based MGs

After the discussions of the NN model including the number of hidden layers, the usage of dropout method, and the sets of the input features, we proceed to perform the multi-objective optimization of Fe-based MGs. In our work, there are 55 decision variables in the multi-objective optimization model. The constraint condition is the total content of constituent elements of alloys, while the boundary condition is controlled by the content of each constituent element. To assess the predictive capability of our multi-objective optimization model, both $Fe_{83}C_1B_xSi_yP_{16-x-y}$ and $Fe_xCo_yNi_{72-x-y}B_{19.2}Si_{4.8}Nb_4$ systems are chosen, because Fe-Si-B system has been reported to have controllable and attractive magnetic properties [6].

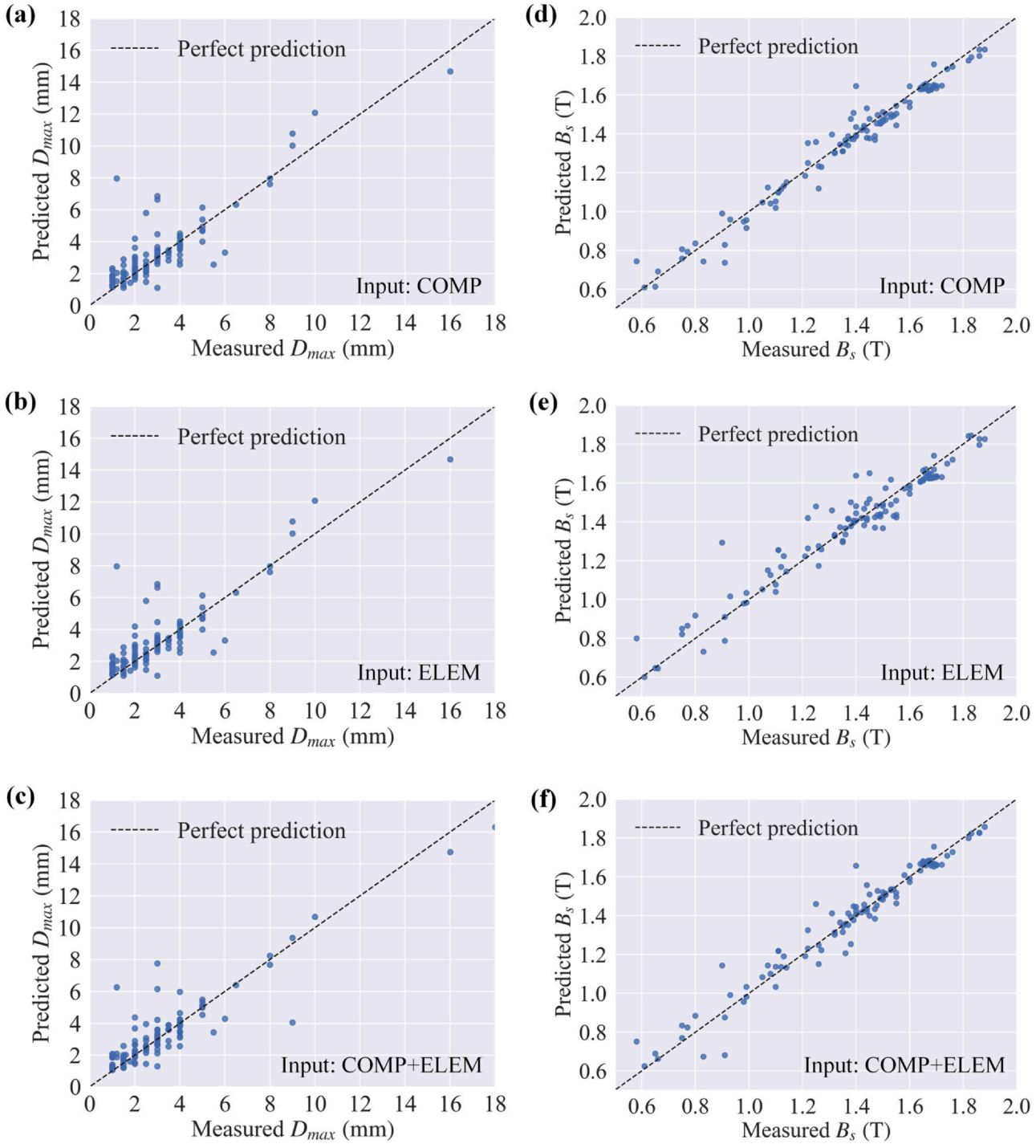

Fig. 7. Predicted (a-c) D_{max} and (d-f) B_s against measured D_{max} and B_s from the different input features including COMP, ELEM, and COMP+ELEM. The diagonal line represents perfect prediction.

Table 3
r^2 and RMSE values of the D_{max} and B_s predictions from three different input features.

Input features	D_{max}		B_s	
	r^2	RMSE (mm)	r^2	RMSE (T)
COMP	0.874	0.895	0.963	0.059
ELEM	0.795	1.140	0.923	0.084
COMP+ELEM	0.817	1.077	0.950	0.068

3.2.1. $Fe_{83}C_1B_xSi_yP_{16-x-y}$ MGs

For $Fe_{83}C_1B_xSi_yP_{16-x-y}$ system, the constraint condition is that the total contents of B, Si, and P elements are 16%. The boundary conditions for each element are as follows:

$$\begin{cases} 0 \le B \le 16\% \\ 0 \le Si \le 16\% \\ 0 \le P \le 16\% \end{cases} \quad (10)$$

In multi-objective optimization, the Pareto front is the set of all Pareto-optimal solutions. The concept allows to restrict attention to the set of optimal choices, and to make tradeoffs within this set,

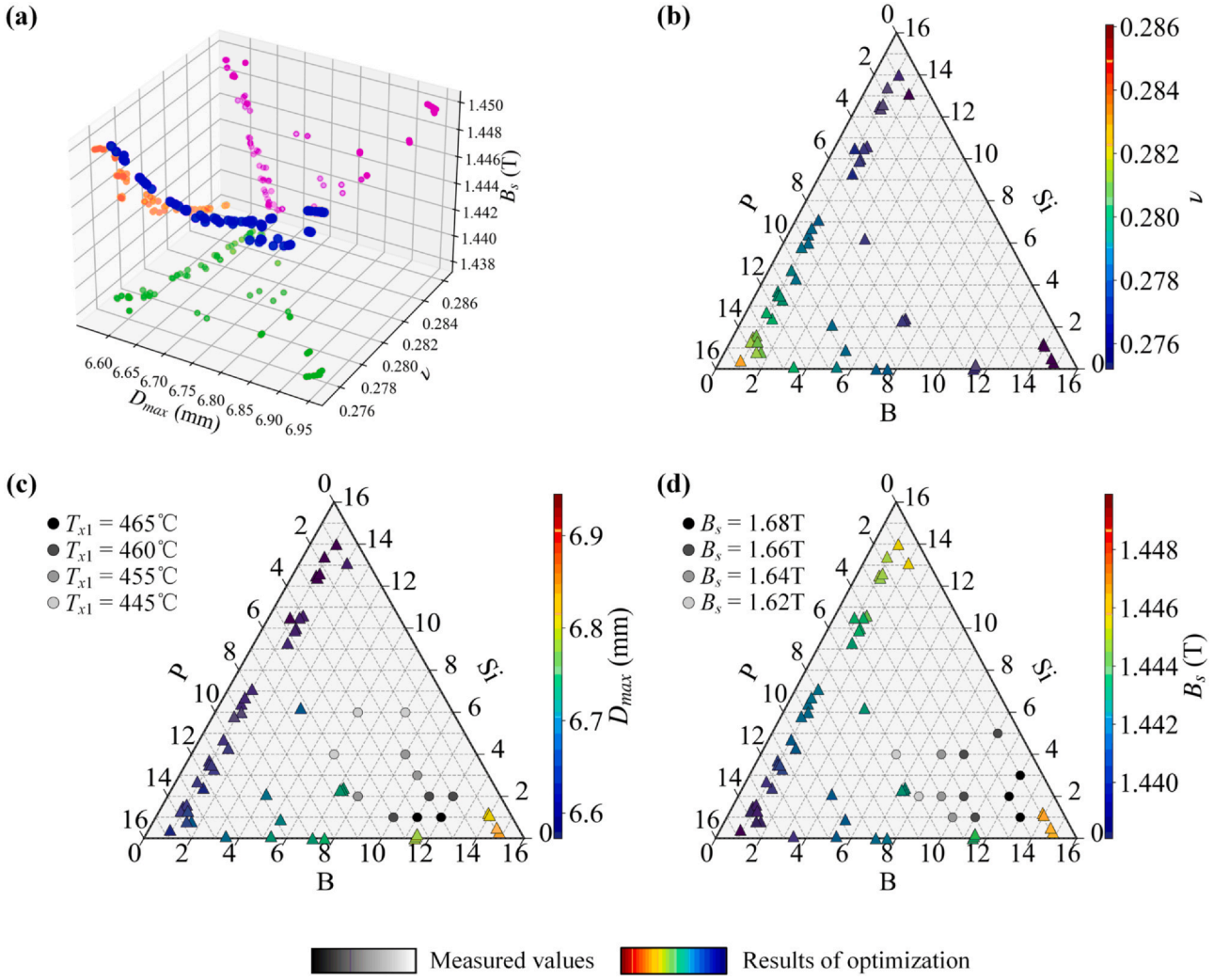

Fig. 8. (a) The Pareto front of $Fe_{83}C_1B_xSi_yP_{16-x-y}$ system. The blue points indicate the target value corresponding to the optimal solution. The orange, green, and pink points represent the projection of the target value onto the three coordinate planes. (b-d) The Pareto-optimal solutions of each objective function for the $Fe_{83}C_1B_xSi_yP_{16-x-y}$ system. The grayscale points are the measured values from experiments.

rather than considering the full range of every parameter. The Pareto front of $Fe_{83}C_1B_xSi_yP_{16-x-y}$ system is plotted in Fig. 8(a). Obviously, it is difficult to simultaneously achieve the optimal values for all objectives. The Pareto-optimal solutions for ν, D_{max}, and B_s, are separately plotted in Fig. 8(b-d). It can be seen that the optimal composition for B_s is close to that for D_{max}. Generally speaking, the GFA and B_s in Fe-based MGs are in conflict with each other. B_s is positively correlated with the Fe content, while the reduced Fe content after the addition of other elements is beneficial for GFA improvement. In our work, the optimal compositions for B_s and D_{max} are very close, which may be due to the fixed Fe content during evolution. Referring to the optimal composition for D_{max} as shown in Fig. 8(c), the content of B element is much higher than those of Si and P elements. Previous studies have reported that the B element is difficult to spread and can inhibit grain growth, which plays a key role in the formation of amorphous phase [70]. In addition, Wang et al. found that an appropriate addition of P element helps to improve the GFA of Fe-B-Si-P system, whereas it deteriorates the GFA and soft magnetic properties once the P element content becomes excessive [22]. For the optimal composition for B_s as shown in Fig. 8(d), the content of P element is low. Since the average magnetic moment is proportional to the average magnetic valence, the metalloids deteriorate saturation magnetization in the order of P > Si > B [13]. This finding is consistent with the results of Williams et al. [71].

Our multi-objective optimization results are consistent with the experimental results of Wang et al. [72]. Wang et al. proposed the crystallization temperature onset (T_{x1}) to reflect the GFA. Our Pareto-optimal results are in good agreement with the distribution of T_{x1}, as shown in Fig. 8(c). It can be observed that the regime of large D_{max} locates at the alloy compositions with more B elements but fewer P and Si elements. It should be noted that the D_{max} values may be overestimated in our work, as the training set is deficient of samples that cannot be cast into MGs. However, this may not change the choice of the Pareto-optimal alloys. For B_s prediction, the Pareto-optimal results are close to the experimental results except for the upper corner of Fig. 8(d). However, the Pareto-optimal alloys located in this area have relatively lower GFA as indicated in Fig. 8(c).

3.2.2. The $Fe_xCo_yNi_{72-x-y}B_{19.2}Si_{4.8}Nb_4$ alloy system

For $Fe_xCo_yNi_{72-x-y}B_{19.2}Si_{4.8}Nb_4$ system, the constraint condition is that the total contents of Fe, Co, and Ni elements are 72%. The boundary conditions for each element are as follows:

$$\begin{cases} 0 \le \text{Fe} \le 72\% \\ 0 \le \text{Co} \le 72\% \\ 0 \le \text{Ni} \le 72\% \end{cases} \tag{11}$$

Fig. 9(a) shows the Pareto front for $Fe_xCo_yNi_{72-x-y}B_{19.2}Si_{4.8}Nb_4$ system. In view of the orthographic projections of Pareto front on

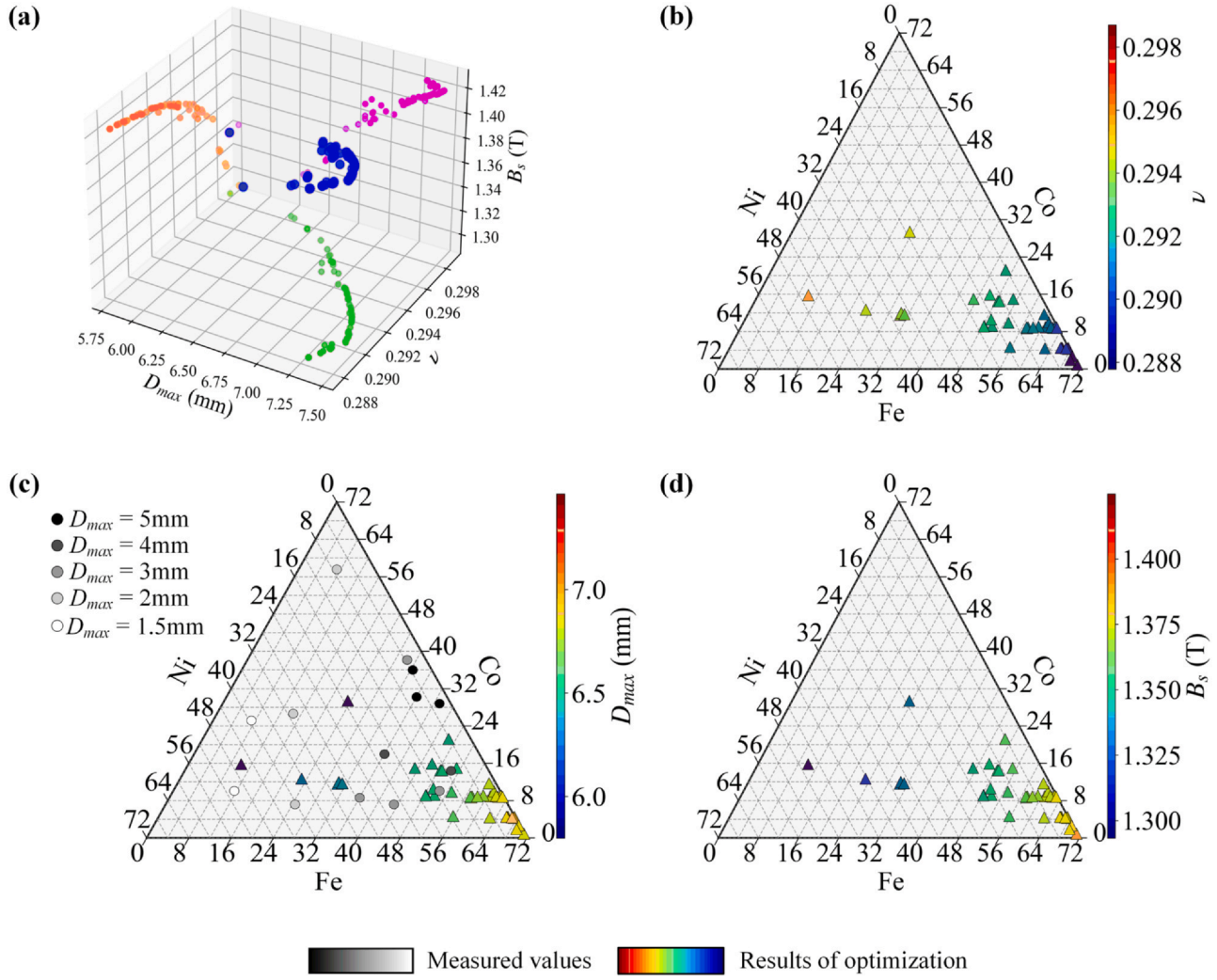

Fig. 9. (a) The Pareto front of $Fe_xCo_yNi_{72-x-y}B_{19.2}Si_{4.8}Nb_4$ system. The blue points indicate the target value corresponding to the optimal solution. The orange, green, and pink points represent the projection of the target value onto the three coordinate planes. (b-d) The Pareto-optimal solution of each objective function for the $Fe_xCo_yNi_{72-x-y}B_{19.2}Si_{4.8}Nb_4$ system. The grayscale points are the measured values from experiments.

each coordinate plane, it is observed that the two objectives of D_{max} and B_s can reach the optimal values simultaneously. This can be attributed to the fact that the contents of elements related to GFA (i.e., B, Si, and Nb) remain unchanged during optimization. The optimal compositions of D_{max} and B_s shown in Fig. 9(c-d) are almost the same, located on the regions with high content of Fe and low contents of Co and Ni. Due to the lower magnetic moment of Ni and the paramagnetism associated with γ-FeNi, the addition of Ni can reduce the B_s [73]. It should be pointed out that our optimization results of D_{max} are consistent with the work of Inoue et al. [74]. For the optimal compositions of plasticity shown in Fig. 9(b), the Ni content increases with ν and is much higher than those of Fe and Co elements. Previous studies have reported that a moderate amount of Ni can improve the plasticity of Fe-based MGs [18]. The substitution of Ni can retain the γ-FeNi short-order atomic arrangement, which is one of the origins of good plasticity in Fe-Ni-based MGs [13,75].

Before concluding, it is instructive to discuss the generality of our approach. Although the multi-objective optimization approach proposed in this study has shown great potential in finding new Fe-based MGs, it still has some limitations to be clarified. First of all, the available dataset for Fe-based MGs is insufficient, especially the ν values. More data will certainly increase the accuracy of our ML model. Besides, the NN model for predicting GFA may overestimate the D_{max} values, because the dataset does not take into account samples that cannot be cast into MGs. In addition, the criterion of ν for plasticity in MGs lacks versatility [38]. Finally, the shear moduli of metalloid elements are assumed, which may affect the accuracy of ν.

4. Conclusions

The search for high-performance Fe-based MGs is very important for their commercial applications. Although the rapid progresses in ML approach to predict the individual property of MGs, it is still challenging for multi-objective optimization. In this study, we have presented a hybrid ML framework based on NN which models the objective functions, in combination with GA to enable the optimization of conflicting material properties. The influences of the number of hidden layers, dropout method, and input features on the NN prediction accuracy are systematically investigated. Our results reveal that the dropout method can improve the model performance, and more hidden layers are required to predict D_{max} due to the skewed data distribution. Moreover, the use of alloy composition as sole input can achieve better prediction performance, compared with the input of the elemental properties or the combination of alloy composition and elemental properties. D_{max} and B_s are well predicted with high r^2 values of 0.874 and 0.963, respectively. We finally validate this ML framework on the $Fe_{83}C_1B_xSi_yP_{16-x-y}$ and

$Fe_xCo_yNi_{72-x-y}B_{19.2}Si_{4.8}Nb_4$ systems, with predictions achieving a good agreement with the experimental results. This paper thus provides insights on the optimization of multi-objective problems towards the design of Fe-based MGs for advanced multifunctional applications.

CRediT authorship contribution statement

Y.X. Zhang: Investigation, Formal analysis, Visualization, Writing - original draft. **S.J. Xie:** Investigation, Visualization. **W. Guo:** Investigation, Visualization. **J. Ding:** Investigation. **L.H. Poh:** Writing - review & editing, Supervision. **Z.D. Sha:** Conceptualization, Writing - review & editing, Supervision.

Data Availability

Data will be made available on request.

Declaration of Competing Interest

The authors declare that they have no known competing financial interests or personal relationships that could have appeared to influence the work reported in this paper.

Acknowledgements

The authors would like to acknowledge financial support from the National Natural Science Foundation of China (No. 11972278) and the opening fund of the State Key Laboratory of Nonlinear Mechanics.

References

[1] W.H. Wang, Bulk metallic glasses with functional physical properties, Adv. Mater. 21 (2009) 4524–4544, https://doi.org/10.1002/adma.200901053
[2] A.L. Greer, E. Ma, Bulk metallic glasses: At the cutting edge of metals research, MRS Bull. 32 (2007) 611–619, https://doi.org/10.1557/mrs2007.121
[3] M.F. Ashby, A.L. Greer, Metallic glasses as structural materials, Scr. Mater. 54 (2006) 321–326, https://doi.org/10.1016/j.scriptamat.2005.09.051
[4] A. Inoue, Bulk glassy alloys: Historical development and current research, Engineering 1 (2015) 54–66, https://doi.org/10.15302/J-ENG-2015038
[5] Y. Yoshizawa, S. Oguma, K. Yamauchi, New Fe-based soft magnetic alloys composed of ultrafine grain structure, J. Appl. Phys. 64 (1988) 6044–6046, https://doi.org/10.1063/1.342149
[6] K.F. Yao, L.X. Shi, S.Q. Chen, N. Shao, N. Chen, J.L. Jia, Research progress and application prospect of Fe-based soft magnetic amorphous/nanocrystalline alloys, Acta Phys. Sin. 67 (2018) 016101, , https://doi.org/10.7498/aps.67.20171473
[7] K. Suzuki, A. Makino, A. Inoue, T. Masumoto, Soft magnetic properties of nanocrystalline bcc Fe-Zr-B and Fe-M-B-Cu (M=transition metal) alloys with high saturation magnetization, J. Appl. Phys. 70 (1991) 6232–6237, https://doi.org/10.1063/1.350006
[8] M.E. McHenry, M.A. Willard, D.E. Laughlin, Amorphous and nanocrystalline materials for applications as soft magnets, Prog. Mater. Sci. 44 (1999) 291–433, https://doi.org/10.1016/S0079-6425(99)00002-X
[9] A. Inoue, T. Zhang, T. Masumoto, Glass-forming ability of alloys, J. Non Cryst. Solids 156–158 (1993) 473–480, https://doi.org/10.1016/0022-3093(93)90003-G
[10] H.S. Chen, Glassy metals, Rep. Prog. Phys. 43 (1980) 353–432, https://doi.org/10.1088/0034-4885/43/4/001
[11] M.W. Chen, A brief overview of bulk metallic glasses, NPG Asia Mater. 3 (2011) 82–90, https://doi.org/10.1038/asiamat.2011.30
[12] L.X. Shi, X.Y. Hu, Y.H. Li, G.T. Yuan, K.F. Yao, The complementary effects of Fe and metalloids on the saturation magnetization of Fe-based amorphous alloys, Intermetallics 131 (2021) 107116, , https://doi.org/10.1016/j.intermet.2021.107116
[13] H.X. Li, Z.C. Lu, S.L. Wang, Y. Wu, Z.P. Lu, Fe-based bulk metallic glasses: Glass formation, fabrication, properties and applications, Prog. Mater. Sci. 103 (2019) 235–318, https://doi.org/10.1016/j.pmatsci.2019.01.003
[14] M. Mitera, T. Masumoto, N.S. Kazama, Effect of silicon addition on the magnetic properties of Fe-B-C amorphous alloys, J. Appl. Phys. 50 (1979) 7609–7611, https://doi.org/10.1063/1.326860
[15] A.D. Wang, Q.K. Man, M.X. Zhang, H. Men, B.L. Shen, S.J. Pang, T. Zhang, Effect of B to P concentration ratio on glass-forming ability and soft-magnetic properties in [(Fe0.5Ni0.5)0.78B0.22−xPx]97Nb3 glassy alloys, Intermetallics 20 (2012) 93–97, https://doi.org/10.1016/j.intermet.2011.08.020
[16] D.S. Sun, S.M. Hong, H.M. Jin, L. Jin, C.G. Kim, C.O. Kim, Effect of P addition on microstructure and soft magnetic properties of Fe(73.5−x)Nb3Cu1PxSi13.5B9 alloys, J. Magn. Magn. Mater. 304 (2006) e198–e200, https://doi.org/10.1016/j.jmmm.2006.01.160
[17] J. Zhou, Q.Q. Wang, X.D. Hui, Q.S. Zeng, Y.W. Xiong, K. Yin, B. Sun, L. Sun, M. Stoica, W. Wang, B. Shen, A novel FeNi-based bulk metallic glass with high notch toughness over 70 MPa m1/2 combined with excellent soft magnetic properties, Mater. Des. 191 (2020) 108597, , https://doi.org/10.1016/j.matdes.2020.108597
[18] J. Zhou, B.A. Sun, Q.Q. Wang, Q.M. Yang, W.M. Yang, B.L. Shen, Effects of Ni and Si additions on mechanical properties and serrated flow behavior in FeMoPCB bulk metallic glasses, J. Alloy. Compd. 783 (2019) 555–564, https://doi.org/10.1016/j.jallcom.2018.12.331
[19] H. Zheng, L. Zhu, S.S. Jiang, Y.G. Wang, S.N. Liu, S. Lan, F.G. Chen, Role of Ni and Co in tailoring magnetic and mechanical properties of Fe84Si2B13P1 metallic glass, J. Alloy. Compd. 816 (2020) 152549, , https://doi.org/10.1016/j.jallcom.2019.152549
[20] J. Xu, Y.Z. Yang, W. Li, Z.W. Xie, X.C. Chen, Effect of the substitution of C for Si on microstructure, magnetic properties and bending ductility in high Fe content FeSiBCuPC alloy ribbons, J. Alloy. Compd. 727 (2017) 610–615, https://doi.org/10.1016/j.jallcom.2017.08.181
[21] J. Xu, Y.Z. Yang, W. Li, X.C. Chen, Z.W. Xie, Effect of P addition on glass forming ability and soft magnetic properties of melt-spun FeSiBCuC alloy ribbons, J. Magn. Magn. Mater. 417 (2016) 291–293, https://doi.org/10.1016/j.jmmm.2016.05.103
[22] C.J. Wang, A.N. He, A.D. Wang, J. Pang, X.F. Liang, Q. Li, C. Chang, K. Qiu, X. Wang, Effect of P on glass forming ability, magnetic properties and oxidation behavior of FeSiBP amorphous alloys, Intermetallics 84 (2017) 142–147, https://doi.org/10.1016/j.intermet.2016.12.024
[23] L. Cui, H. Men, A. Makino, T. Kubota, K. Yubuta, M. Qi, A. Inoue, Effect of Cu and P on the crystallization behavior of Fe-rich hetero-amorphous FeSiB alloy, Mater. Trans. 50 (2009) 2515–2520, https://doi.org/10.2320/matertrans.M2009206
[24] Y.L. Liu, C. Niu, Z. Wang, Y. Gan, Y. Zhu, S.H. Sun, T. Shen, Machine learning in materials genome initiative: A review, J. Mater. Sci. Technol. 57 (2020) 113–122, https://doi.org/10.1016/j.jmst.2020.01.067
[25] K.T. Butler, D.W. Davies, H. Cartwright, O. Isayev, A. Walsh, Machine learning for molecular and materials science, Nature 559 (2018) 547–555, https://doi.org/10.1038/s41586-018-0337-2
[26] Q. Zhou, S. Lu, Y. Wu, J. Wang, Property-oriented material design based on a data-driven machine learning technique, J. Phys. Chem. Lett. 11 (2020) 3920–3927, https://doi.org/10.1021/acs.jpclett.0c00665
[27] F. Ren, L. Ward, T. Williams, K.J. Laws, C. Wolverton, J. Hattrick-Simpers, A. Mehta, Accelerated discovery of metallic glasses through iteration of machine learning and high-throughput experiments, Sci. Adv. 4 (2018) eaaq1566, https://doi.org/10.1126/sciadv.aaq1566
[28] L. Ward, S.C. Okeeffe, J. Stevick, G.R. Jelbert, M. Aykol, C. Wolverton, A machine learning approach for engineering bulk metallic glass alloys, Acta Mater. 159 (2018) 102–111, https://doi.org/10.1016/j.actamat.2018.08.002
[29] L. Ward, A. Agrawal, A. Choudhary, C. Wolverton, A general-purpose machine learning framework for predicting properties of inorganic materials, NPJ Comput. Mater. 2 (2016) 16028, https://doi.org/10.1038/npjcompumats.2016.28
[30] Y.T. Sun, H.Y. Bai, M.Z. Li, W.H. Wang, Machine learning approach for prediction and understanding of glass-forming ability, J. Phys. Chem. Lett. 8 (2017) 3434–3439, https://doi.org/10.1021/acs.jpclett.7b01046
[31] A.H. Cai, X. Xiong, Y. Liu, W.K. An, G.J. Zhou, Y. Luo, T.L. Li, X.S. Li, X.F. Tan, Compositional optimization of glass forming alloys based on critical dimension by using artificial neural network, Trans. Nonferrous Met. Soc. China 24 (2014) 1458–1466, https://doi.org/10.1016/S1003-6326(14)63213-1
[32] D. Liu, K. Guo, F.W. Tang, F. Mao, X.M. Liu, C. Hou, H. Wang, H. Lu, X. Song, Selecting doping elements by data mining for advanced magnets, Chem. Mater. 31 (2019) 10117–10125, https://doi.org/10.1021/acs.chemmater.9b03379
[33] Z.C. Lu, X. Chen, X.J. Liu, D.Y. Lin, Y. Wu, Y. Zhang, H. Wang, S. Jiang, H. Li, X. Wang, Z. Lu, Interpretable machine-learning strategy for soft-magnetic property and thermal stability in Fe-based metallic glasses, Npj Comput. Mater. 6 (2020) 187, https://doi.org/10.1038/s41524-020-00460-x
[34] F. Yang, Z. Li, Q. Wang, B.B. Jiang, B.J. Yan, P. Zhang, W. Xu, C. Dong, P.K. Liaw, Cluster-formula-embedded machine learning for design of multicomponent β-Ti alloys with low Young's modulus, Npj Comput. Mater. 6 (2020) 101, https://doi.org/10.1038/s41524-020-00372-w
[35] D.G. Mastropietro, J.A. Moya, Design of Fe-based bulk metallic glasses for maximum amorphous diameter (Dmax) using machine learning models, Comput. Mater. Sci. 188 (2021) 110230, , https://doi.org/10.1016/j.commatsci.2020.110230
[36] J. Xiong, S.Q. Shi, T.Y. Zhang, Machine learning prediction of glass-forming ability in bulk metallic glasses, Comput. Mater. Sci. 192 (2021) 110362, , https://doi.org/10.1016/j.commatsci.2021.110362
[37] M. Samavatian, R. Gholamipour, V. Samavatian, Discovery of novel quaternary bulk metallic glasses using a developed correlation-based neural network approach, Comput. Mater. Sci. 186 (2021) 110025, , https://doi.org/10.1016/j.commatsci.2020.110025
[38] S.J. Wu, Z.Q. Liu, R.T. Qu, Z.F. Zhang, Designing metallic glasses with optimal combinations of glass-forming ability and mechanical properties, J. Mater. Sci. Technol. 67 (2021) 254–264, https://doi.org/10.1016/j.jmst.2020.08.028
[39] G. Dhiman, A. Kaur, Optimizing the design of airfoil and optical buffer problems using spotted hyena optimizer, Designs 2 (2018) 28, https://doi.org/10.3390/designs2030028
[40] M. García-Carrillo, A.B. Espinoza-Martínez, L.F. Ramos-de Valle, S. Sánchez-Valdés, Simultaneous optimization of thermal and electrical conductivity of high density polyethylene-carbon particle composites by artificial neural networks and multi-objective genetic algorithm, Comput. Mater. Sci. 201 (2022) 110956, , https://doi.org/10.1016/j.commatsci.2021.110956

[41] G. Cybenko, Approximation by superpositions of a sigmoidal function, Math. Control Signal Syst. 2 (1989) 303–314, https://doi.org/10.1007/BF02551274
[42] V. Nair, G.E. Hinton, Rectified linear units improve restricted boltzmann machines, in: Haifa, 2010: pp. 807–814.
[43] X. Glorot, A. Bordes, Y. Bengio, Deep sparse rectifier neural networks, in: AISTATS, 2010: p. 10.
[44] N. Srivastava, G. Hinton, A. Krizhevsky, I. Sutskever, R. Salakhutdinov, Dropout: a simple way to prevent neural networks from overfitting, J. Mach. Learn. Res 15 (2014) 1929–1958.
[45] J.O. Rawlings, S.G. Pantula, D.A. Dickey, Applied Regression Analysis: A Research Tool, 2nd ed.,, Springer,, New York, 1998.
[46] J.J. Lewandowski, W.H. Wang, A.L. Greer, Intrinsic plasticity or brittleness of metallic glasses, Philos. Mag. Lett. 85 (2005) 77–87, https://doi.org/10.1080/09500830500080474
[47] J.J. Lewandowski, M. Shazly, A. Shamimi Nouri, Intrinsic and extrinsic toughening of metallic glasses, Scr. Mater. 54 (2006) 337–341, https://doi.org/10.1016/j.scriptamat.2005.10.010
[48] W.H. Wang, The elastic properties, elastic models and elastic perspectives of metallic glasses, Prog. Mater. Sci. 57 (2012) 487–656, https://doi.org/10.1016/j.pmatsci.2011.07.001
[49] Z.Q. Liu, R.F. Wang, R.T. Qu, Z.F. Zhang, Precisely predicting and designing the elasticity of metallic glasses, J. Appl. Phys. 115 (2014) 203513, , https://doi.org/10.1063/1.4880337
[50] Jazzbin, Geatpy: The genetic and evolutionary algorithm toolbox with high performance in python, (2020). ⟨http://geatpy.com⟩ (accessed December 22, 2021).
[51] K. Deb, A. Pratap, S. Agarwal, T. Meyarivan, A fast and elitist multiobjective genetic algorithm: NSGA-II, IEEE Trans. Evol. Comput. 6 (2002) 182–197, https://doi.org/10.1109/4235.996017
[52] H. Jain, K. Deb, An evolutionary many-objective optimization algorithm using reference-point based nondominated sorting approach, part II: handling constraints and extending to an adaptive approach, IEEE Trans. Evol. Comput. 18 (2014) 602–622, https://doi.org/10.1109/TEVC.2013.2281534
[53] Y.J. Wei, X.Q. Lei, L.S. Huo, W.H. Wang, A.L. Greer, Towards more uniform deformation in metallic glasses: The role of Poisson's ratio, Mater. Sci. Eng. A 560 (2013) 510–517, https://doi.org/10.1016/j.msea.2012.09.096
[54] G.R. Garrett, M.D. Demetriou, J. Chen, W.L. Johnson, Effect of microalloying on the toughness of metallic glasses, Appl. Phys. Lett. 101 (2012) 241913, , https://doi.org/10.1063/1.4769997
[55] B.Y. Ren, Z.L. Long, R.J. Deng, A new criterion for predicting the glass-forming ability of alloys based on machine learning, Comput. Mater. Sci. 189 (2021) 110259, , https://doi.org/10.1016/j.commatsci.2020.110259
[56] M.Q. Jiang, L.H. Dai, Intrinsic correlation between fragility and bulk modulus in metallic glasses, Phys. Rev. B 76 (2007) 054204, , https://doi.org/10.1103/PhysRevB.76.054204
[57] J.L. Gu, Y. Shao, K.F. Yao, The novel Ti-based metallic glass with excellent glass forming ability and an elastic constant dependent glass forming criterion, Materialia 8 (2019) 100433, , https://doi.org/10.1016/j.mtla.2019.100433
[58] J. Xiong, T.Y. Zhang, S.Q. Shi, Machine learning prediction of elastic properties and glass-forming ability of bulk metallic glasses, MRS Commun. 9 (2019) 576–585, https://doi.org/10.1557/mrc.2019.44
[59] Z.Z. Yuan, S.L. Bao, Y. Lu, D.-P. Zhang, L. Yao, A new criterion for evaluating the glass-forming ability of bulk glass forming alloys, J. Alloy. Compd. 459 (2008) 251–260, https://doi.org/10.1016/j.jallcom.2007.05.037
[60] A.H. Cai, H. Chen, W.K. An, J.Y. Tan, Y. Zhou, Relationship between melting enthalpy ΔHm and critical cooling rate Rc for bulk metallic glasses, Mater. Sci. Eng. A 457 (2007) 6–12, https://doi.org/10.1016/j.msea.2007.01.140
[61] J. Schroers, W.L. Johnson, Ductile bulk metallic glass, Phys. Rev. Lett. 93 (2004) 255506, , https://doi.org/10.1103/PhysRevLett.93.255506
[62] H.B. Yu, P. Yu, W.H. Wang, H.Y. Bai, Thulium-based bulk metallic glass, Appl. Phys. Lett. 92 (2008) 141906, , https://doi.org/10.1063/1.2908047
[63] J.J. Lewandowski, X.J. Gu, A. Shamimi Nouri, S.J. Poon, G.J. Shiflet, Tough Fe-based bulk metallic glasses, Appl. Phys. Lett. 92 (2008) 091918, , https://doi.org/10.1063/1.2890489
[64] Y. Kawazoe, J.Z. Yu, A.P. Tsai, T. Masumoto, Nonequilibrium Phase Diagrams of Ternary Amorphous Alloys, Springer-Verlag,, Berlin, 1997, https://doi.org/10.1007/b58222
[65] Q. Jiang, B.Q. Chi, J.C. Li, A valence electron concentration criterion for glass-formation ability of metallic liquids, Appl. Phys. Lett. 82 (2003) 2984–2986, https://doi.org/10.1063/1.1571984
[66] Y.X. Zhang, G.C. Xing, Z.D. Sha, L.H. Poh, A two-step fused machine learning approach for the prediction of glass-forming ability of metallic glasses, J. Alloy. Compd. 875 (2021) 160040, , https://doi.org/10.1016/j.jallcom.2021.160040
[67] B.H. Deng, Y.L. Zhang, Critical feature space for predicting the glass forming ability of metallic alloys revealed by machine learning, Chem. Phys. 538 (2020) 110898, , https://doi.org/10.1016/j.chemphys.2020.110898
[68] J. Xiong, S.Q. Shi, T.Y. Zhang, A machine-learning approach to predicting and understanding the properties of amorphous metallic alloys, Mater. Des. 187 (2020) 108378, , https://doi.org/10.1016/j.matdes.2019.108378
[69] X. Li, G. Shan, C.H. Shek, Machine learning prediction of magnetic properties of Fe-based metallic glasses considering glass forming ability, J. Mater. Sci. Technol. 103 (2022) 113–120, https://doi.org/10.1016/j.jmst.2021.05.076
[70] Y.X. Geng, Y.M. Wang, Z. Wang, J.B. Qiang, H.B. Wang, C. Dong, O. Tegus, Formation and structure-property correlation of new bulk Fe–B–Si–Hf metallic glasses, Mater. Des. 106 (2016) 69–73, https://doi.org/10.1016/j.matdes.2016.05.102
[71] A. Williams, V. Moruzzi, A. Malozemoff, K. Terakura, Generalized slater-pauling curve for transition-metal magnets, IEEE Trans. Magn. 19 (1983) 1983–1988, https://doi.org/10.1109/TMAG.1983.1062706
[72] A.D. Wang, C. Zhao, H. Men, A.N. He, C.T. Chang, X.M. Wang, R.W. Li, Fe-based amorphous alloys for wide ribbon production with high Bs and outstanding amorphous forming ability, J. Alloy. Compd. 630 (2015) 209–213, https://doi.org/10.1016/j.jallcom.2015.01.056
[73] I. Bakonyi, Relevance of Fe atomic volumes for the magnetic properties of Fe-rich metallic glasses, J. Magn. Magn. Mater. 324 (2012) 3961–3965, https://doi.org/10.1016/j.jmmm.2012.07.003
[74] A. Inoue, B. Shen, A. Takeuchi, Developments and applications of bulk glassy alloys in late transition metal base system, Mater. Trans. 47 (2006) 1275–1285, https://doi.org/10.2320/matertrans.47.1275
[75] B. Sarac, Y.P. Ivanov, A. Chuvilin, T. Schöberl, M. Stoica, Z. Zhang, J. Eckert, Origin of large plasticity and multiscale effects in iron-based metallic glasses, Nat. Commun. 9 (2018) 1333, https://doi.org/10.1038/s41467-018-03744-5